Hindawi
Scientific Programming
Volume 2022, Article ID 8290106, 10 pages
https://doi.org/10.1155/2022/8290106

Research Article

ARM-Based Indoor RGB-LED Visible Light Communication System

Jingjing Bao, Qiang Mai, Zhangwen Fang, and Xiaowen Mao

School of Electronic Information, Dongguan Polytechnic, Guangdong, Dongguan 523808, China

Correspondence should be addressed to Jingjing Bao; baojj@dgpt.edu.cn

Received 21 April 2022; Revised 24 May 2022; Accepted 3 June 2022; Published 18 June 2022

Academic Editor: Lianhui Li

As a new green solid-state light source, semiconductor light-emitting diodes (LEDs) have the advantages of low power consumption, small size, long life, short response time, and good modulation performance. At the same time, the frequency band to which LED light sources belong does not require regulatory registration, thus alleviating the current problem of spectrum scarcity for wireless communications. However, white LED-based visible light communication (VLC) systems suffer from limited bandwidth and low energy efficiency. Therefore, an ARM-based indoor RGB-LED VLC system is proposed. Firstly, the three RGB colours are mixed into white light, thus obtaining a larger modulation bandwidth than normal white LEDs while illuminating normally. Secondly, the S3C6410 processor is used to modulate and demodulate the RGB-LEDs with biased light OFDM, thus obtaining a high spectrum utilisation while ensuring system transmission stability. Then, according to the characteristics of the light source of the VLC system, the leading and window functions used in the optical network transceiver module are designed to improve the communication energy efficiency of the system. Finally, functional tests were carried out on an ARM development board. The experimental results show that with a single RGB-LED light source, the maximum transmission distance is 5 cm, the maximum average delay is 68 ms, the maximum throughput is 25 Mbps, and the BER is controlled below 3.2×10^{-3}, which meets the basic communication requirements.

1. Introduction

With the advent of the 5G era, the demand for mobile data services is growing exponentially, and the available frequency band resources for RF communications are becoming increasingly scarce. As a result, the visible band, which has a huge bandwidth, is rapidly attracting widespread attention. Semiconductor light-emitting diodes (LEDs), as a new green solid-state light source, have the advantages of low power consumption, small size, long life, short response time, and good modulation performance [1–7]. By simply replacing conventional incandescent lamps with LEDs, the lighting can be transformed into a wireless network transmitter. Furthermore, with the development of conventional wireless communication, the limited radio spectrum resources are becoming increasingly prominent, leading to the issue of spectrum resource utilisation becoming very important.

The frequency band to which LED light sources belong does not require regulatory registration and can alleviate the current shortage of spectrum for wireless communication. Therefore, the use of white LED light sources for indoor lighting for VLC is a current research hotspot in the field of wireless communication at home and abroad. VLC is the use of specific modulation techniques to couple the data signals to be transmitted with light-emitting diodes [8–10]. At the same time, a high-speed modulated light wave signal from the LED device is used to transmit the information. The receiver generates an electrical signal based on the strength of the received light signal via a photodetector, and the signal is restored by the signal processing circuit.

LED-based VLC can greatly broaden the communication spectrum range and is one of the feasible solutions to alleviate the tight wireless spectrum resources. Its advantages are mainly reflected in these aspects [11–13]: (1) the data transmission speed is almost the same as that of optical fiber.

Under certain circumstances, it can transmit data at 1 Gbps. (2) VLC is not limited by spectrum. In contrast to RF wireless communication, VLC technology is able to allocate spectrum resources more scientifically. (3) VLC technology is green and environmentally friendly. VLC technology does not cause harm to the human eye and does not cause signal interference and impact on existing systems. (4) Good confidentiality: VLC technology is not easy to be listened to. (5) The cost is relatively low. VLC-related equipment and systems are very simple to deploy and are well compatible with current RF communication systems.

The above advantages show that if VLC technology can be applied to practical production and life, it will help completely solve the problems of spectrum resource constraint and signal interference. This shows that VLC technology has great potential for application. VLC technology can be perfectly integrated with the network access technology of today's homes. By using LED lighting in the average home as a kind of optical routing, it is possible to provide network access to the home.

VLC is a more energy-efficient and environmentally friendly way of accessing the Internet than mainstream Wi-Fi communication today. In addition, VLC can also be used for indoor positioning technology [14]. By collecting and transmitting the location information of indoor users through inherent indoor lighting devices, the precise positioning of moving people in indoor locations can be achieved. In some special spatial environments, such as aircraft, hospitals, and mines, there are a large number of electronic devices that are more sensitive to electromagnetic waves. In order to prevent serious consequences caused by electromagnetic wave interference, the use of electronic communication equipment in these situations is strictly limited. LED-based VLC is a good solution to these problems, as it does not generate electromagnetic interference.

ARM is a microprocessor with high performance and low power consumption and is favoured by the majority of terminal product manufacturers. The development of ARM terminals has become an important force in the development of information technology and the ARM platform has become the platform of choice for product development in people's lives. The implementation of visible light network access on ARM terminals will certainly greatly facilitate the exchange of information between people. Therefore, an ARM-based indoor VLC system is proposed.

2. Related Studies

VLC technology based on white LEDs is able to achieve both lighting and communication functions at a low cost and is suitable for various network access scenarios. Due to its advantages of being free of electromagnetic interference and green [15], VLC technology has attracted widespread attention and support worldwide.

Research work on VLCs first began in Japan. As early as 2000, Keio University in Japan proposed the feasibility of visible light as a light source for indoor lighting and communication [16]. In 2003, a large group of companies and research institutes formed the VLC Consortium (VLCC) with the aim of establishing a set of industry standards applicable to VLC. In 2008, the EU developed and implemented the OMEGA project, whose main objective was to study data applications for home access networks with transmission speeds exceeding 1 Gbis/s [17], which includes VLC.

At present, one of the key technologies for LED VLC is modulation, coding, and demodulation. Currently, most VLC systems use intensity modulation (IM) direct detection systems, and most of the coding methods are binary OOK (on-off keying) codes. Xiao et al. [18] proposed a real-time visible light transmission network based on non-return-to-zero on-off keying modulation (NRZ-OOK) with a transmission rate of 550 Mbit/s. Wang et al. [19] proposed a modulation technique based on phase shift Manchester coding (PS-Manchester) and mixed time-frequency equalisation, which used RGB-LED to achieve a higher transmission rate.

The light-emitting mechanism of white LEDs makes their bandwidth limited. As a result, the transmission rate of VLC networks is not very high in the currently implemented application scenarios. In visible communication systems, the core component of the transmitter module is the white LED, which can be divided into three main types: PC-LED, RGB-LED, and UV-LED. The RGB-LED light source is a monochromatic combination of red, green, and blue light in proportion to demand. As technology has evolved, the scope of RGB-LEDs has expanded to include more than just a mixture of red, green, and blue light, and RGB-LEDs can be used to produce the desired white light by combining multiple colours in the right proportions. For this reason, the majority of current research has focused on the use of PC-LEDs and RGB-LEDs as transmitters in VLCs. As the modulation bandwidth of RGB-LEDs is higher than that of PC-LEDs, RGB-LEDs are used in the network access scheme proposed in this paper.

In addition, because OFDM can effectively combat intersymbol interference caused by multipath propagation; its implementation complexity is much less than that of a single-carrier system using an equaliser. Therefore, the use of OFDM modulation technology has good prospects for development.

To meet the demand for green communication, current wireless communication technologies not only focus on improving transmission efficiency but also pay more attention to energy efficiency. Therefore, a lot of research work has been carried out on energy efficiency in VLC systems. Marshoud et al. [20] discussed the effect of different waveforms and modulation methods on LED energy efficiency in VLC systems. Ferreira et al. [21] came up with a new multiobjective optimisation method that allows flexible switching between energy efficiency and spectral efficiency functions. Chen et al. [22] derived a closed-form expression for the energy efficiency-spectral efficiency in VLC systems assuming that the LEDs operate in the linear region.

With its unique performance, VLC has great application prospects in the future. ARM is a microprocessor with the

advantages of high performance and low power consumption, so this paper attempts to combine ARM technology and VLC technology to study the feasibility of network access based on ARM terminals, bringing into play the advantages of both and providing a hardware implementation method for ARM-based VLC systems. This paper attempts to combine ARM technology and VLC technology to investigate the feasibility of network access based on ARM terminals, exploit the advantages of both, and provide a hardware implementation method for ARM-based VLC systems.

The main objective of this research is to increase the transmission bandwidth of VLC systems and improve LED energy efficiency. This paper proposes an ARM-based indoor RGB-LED VLC system. The main innovations and contributions include: (1) considering the large modulation bandwidth of RGB-LEDs compared to ordinary white LEDs and the advantages of OFDM modulation technology with its strong anti-interference capability and high spectrum utilisation, this study attempts to combine RGB-LEDs with OFDM technology in order to improve the system transmission bandwidth; (2) based on the characteristics of the light source of the OFDM-based VLC system, the leading and window functions used in the optical network transceiver module were designed to improve the communication energy efficiency of the system; and (3) an embedded ARM platform was built for OFDM modulation and demodulation to achieve low-cost network access for visible light systems.

3. VLC System Light Source Characteristics

3.1. Operating Principles and Characteristics of LEDs. The LED is a semiconductor structure with an internal PN junction that enables the conversion between electrical energy and light energy [23–25]. Therefore, like normal PN junctions, LEDs have physical characteristics such as forward conduction and reverse cut-off. When the PN junction is subjected to a forward voltage, the holes in the P region flow to the N region, while the electrons in the N region flow into the P region. In the process of flowing, when the electrons in high-energy state collide with holes, the excess energy is radiated out in the form of light. LED's light-emitting principle is shown in Figure 1. LED's light emission is spontaneous, so its directivity is poor. We can gather the light of LED by external devices to improve the received light power at the receiving end.

This paper uses the solid-state power amplifier (SSPA) model to describe the voltammetric characteristics of LEDs, which are PN junctions made of semiconductor materials and therefore have the same voltammetric characteristics as PN junctions. The forward voltammetric characteristics of LEDs can be expressed as follows:

$$I_F = I_s\left(\frac{qV_F}{enkT} - 1\right), \tag{1}$$

where I_s is the reverse saturation current, q is the electron charge, n is the constant, k is the Boltzmann constant, and T is the thermodynamic temperature.

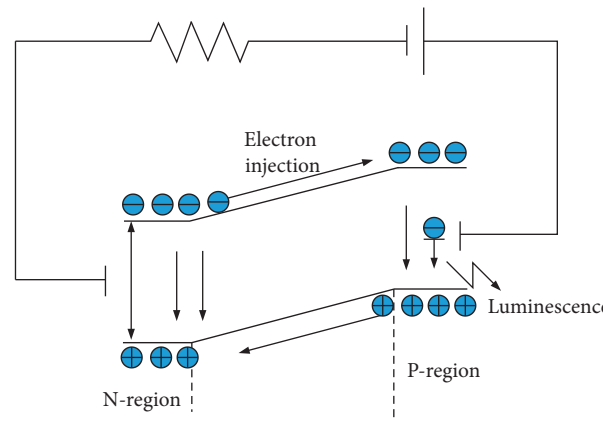

Figure 1: Principle of LED light emission.

The operating voltage of LEDs is divided into four regions, namely the reverse breakdown region, the cut-off region, the start-up region, and the operating region. The start and work zones are the positive zones and are the areas that the system design focuses on. The junction between the start and work zones is the LED turn-on voltage. When the forward voltage is applied to both ends of the LED and the working voltage is less than the starting voltage, the LED cannot normally emit light. At this point, the size of the current through the LED is zero. The working voltage of the LED is slowly increased. When the working voltage exceeds the starting voltage, the LED normally emits light. If we apply the reverse voltage to the LED, the LED is in the cut-off zone. If we continue to increase the reverse voltage, it is likely that the PN junction of the LED will be broken down by the reverse voltage. At this point, the critical voltage that breaks through the LED is called the breakdown voltage. When designing the transmitter circuit of a VLC system, we need to design the modulation circuit or signal coupling circuit according to the operating current of the LED.

3.2. Principle and Characteristics of the Receiving LED. For VLC receiver modules, the core device is the photodetector (PD). Photoelectric detection converts light signals into electrical signals by means of the photoelectric effect between substances. By using photodetection, the receiver can smoothly convert the received visible light signal into an electrical signal that can be recognised by the subsequent signal processing circuit. Currently, the most used photodetectors are positive-intrinsic-negative (PIN) photodiodes, avalanche photodiodes (APD), and image sensors [26].

In a multiuser scenario, each user needs a receiver to receive the signal. Although APDs are more sensitive and support a larger bandwidth, cost considerations led this study to use a PIN photodiode as the receiver. The photoreceiver used in the experiments is a silicon PIN photodiode S10784 from Hamamatsu, Japan. The S10784 has a peak wavelength of 660 nm or 780 nm, as well as a fast response time and high sensitivity. The detailed parameters of the silicon PIN S10784 are shown in Table 1.

Table 1: Silicon PIN S10784 parameters.

Parameters	Numerical values
Light-sensitive area	3.0 mm^2
Pixel count	1
Maximum reverse bias voltage	20 V
Spectral response range	340~1,040 nm
Peak wavelength	760 nm
Sensitivity	0.51 A/W
Dark current	1,000 pA
Cut-off frequency	250 MHz
Junction capacitance	4.5 pF

4. RGB-LED VLC Principle

4.1. Structure and Principle of RGB-LED. VLC technology uses high-speed signals emitted by LEDs to transmit data. This high-speed signal cannot be recognised by the human eye. On the transmitter side, the process of flashing light and dark LEDs at high speed is the process of sending the information. For example, "light" means "1," and "dark" means "0." At the receiving end, the light and dark signals are detected by a corresponding photoelectric detection device. After a series of amplification, filtering, shaping, and other processing, together with mathematical analysis and transformation methods, the information sent by the transmitter can be translated using decoding.

There are two general approaches to white LED formation [27]: PC-LED and RGB-LED. The basic structure of PC-LED is shown in Figure 2. RGB-LED produces the desired white light by mixing the various colours of light, as shown in Figure 3. By mixing the three colours of light at a certain power level, the white light perceived by the human eye is obtained. This method requires a certain electronic circuit to control the mixing ratio of these light colours. Although complex, this method provides the flexibility to obtain the desired light colour with high quantum efficiency.

The colour rendering and radiant luminous efficacy of the RGB-LED are influenced by the three lamps together. In order to make it as close to white as possible, $Ra > 80$ is required and the coordinates ($x = 0.33$ and $y = 0.33$) are satisfied. After several patchwork proportioning tests, the ratio of the three RGB colours was found to be 1:1.2:1. The specific proportioning data are shown in Table 2.

4.2. Solution Design for the Transmitter Side of RGB-LED VLC Systems. The transmitter side of the RGB-LED-based VLC system designed in this paper consists of an RGB-LED light source module, an RGB-LED driver module, a modulation module, and an adder-coupling module. The adder couples the RGB-LED DC drive voltage with the modulating voltage signal from the signal modulation module, which drives the RGB-LED light source module to emit a light signal loaded with useful information. A schematic diagram of the operation of the transmitter is shown in Figure 4.

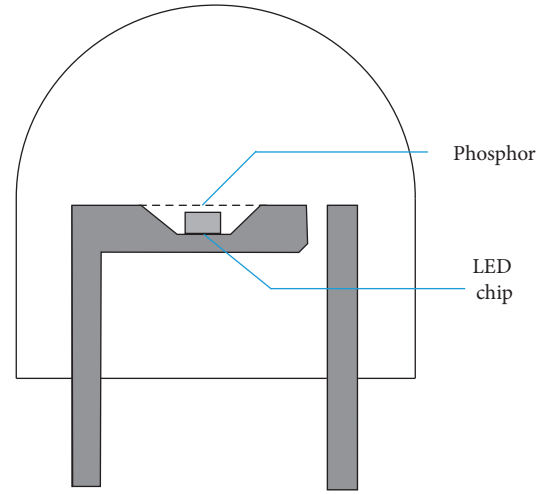

Figure 2: Basic structure of the PC-LED.

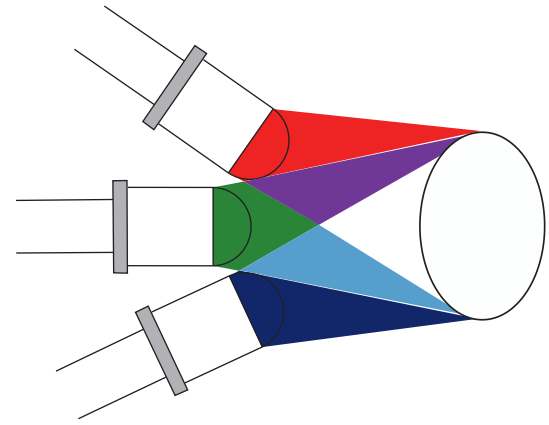

Figure 3: Basic structure of the RGB-LED.

5. ARM-Based Indoor RGB-LED VLC System Design

5.1. Geometric Model for Indoor VLC. Unlike traditional communication theory, the channel model in VLC is closely related to the light source, the channel, and the receiver. In this paper, only the direct line of sight (LOS) link between a single LED and a single PD is considered, and the geometrical scenarios for different layouts of indoor LEDs are considered, as shown in Figure 5. In a VLC system, the LOS optical channel can be well described by its DC gain. The channel DC gain g is defined as follows:

$$g = \frac{(m+1)A_{p\,d}}{2\pi d^2}\cos^m(\varphi)\cos(\theta)T(\theta)G(\theta), \quad (2)$$

where m is the Lambert emission coefficient, $A_{p\,d}$ represents the effective area of the PD, φ is the angle of light emission, θ is the angle of light incidence, and $T(\theta)$ and $G(\theta)$ represent the gain of the optical filter and concentrator, respectively.

5.2. Biased Optical OFDM Modulation Scheme. In this paper, the biased optical OFDM modulation technique is applied to a VLC system. Firstly, the input binary bit stream is

Table 2: RGB trichromatic white LED ratios.

LED	Wavelength (nm)	Spectral bandwidth	Radiant light effect	Energy (W)	Luminous flux
Red	614	20	311.6	1	311.6
Green	546	30	640.9	1.2	769.1
Blue	465	20	54.5	1	54.5

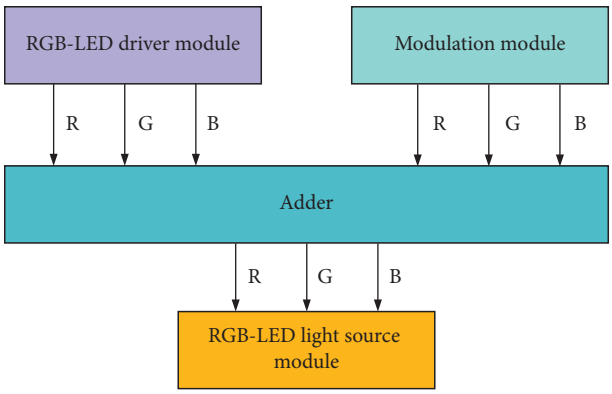

Figure 4: Diagram of the system on the sending end.

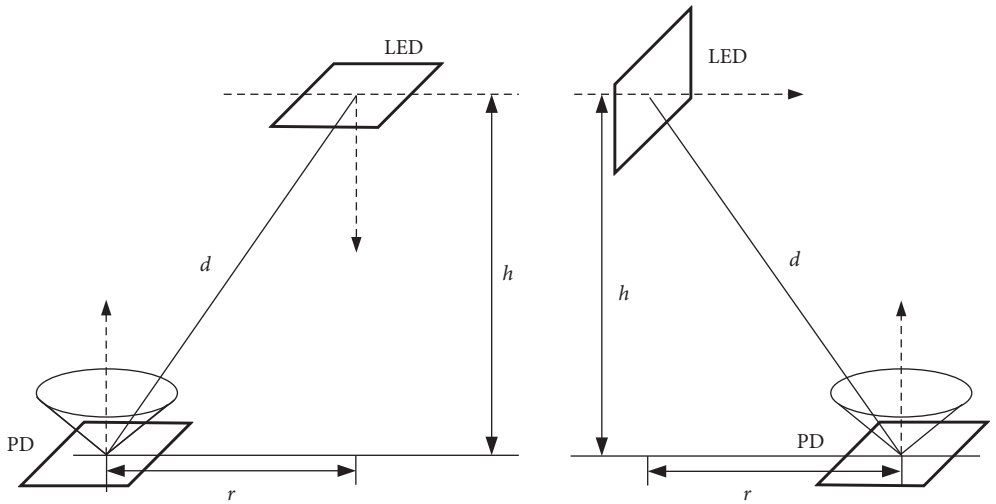

Figure 5: Geometric scene with different layouts of indoor LEDs.

modulated by QAM. Secondly, Hermitian symmetry is performed to obtain a frequency domain complex signal as follows:

$$X = \left[X_0, X_1, \cdots, X_{N/2-1}, X_{N/2}, X^*_{N/2-1}, \cdots, X^*_1\right]^T. \quad (3)$$

The Hermitian symmetry operation performed after QAM modulation is to ensure that the signal after the inverse fast Fourier transform (IFFT) operation is a real-valued signal. Without loss of generality, the real-valued OFDM symbol $x_u(n)$ can be expressed as follows:

$$x_u(n) = \sum_{k=0}^{N-1} \frac{X_k}{\sqrt{N}} e^{j2\pi nk/N}, \quad 0 < n < N-1, \quad (4)$$

where N is the total number of subcarriers.

In general, the DC bias voltage x_{DC} is defined as shown as follows [28]:

$$x_{DC} = \frac{U_{TOV} + U_{\max}}{2}, \quad (5)$$

where U_{TOV} is the LED turn-on voltage and $U_{\max}$ is the maximum DC voltage of the LED. After superimposing the DC bias voltage on $x_u(n)$, a positive real-valued signal $x(n)$ is obtained as follows:

$$x(n) = x_{\mathrm{u}}(n) + x_{\mathrm{DC}}. \quad (6)$$

The output signal via the LED $y(n)$ can be expressed as follows:

$$y(n) = \frac{f(v_{\mathrm{LED}})}{\left(1 + \left(f(v_{\mathrm{LED}})/i_{\max}\right)^{2t}\right)^{1/2t}}, \quad (7)$$

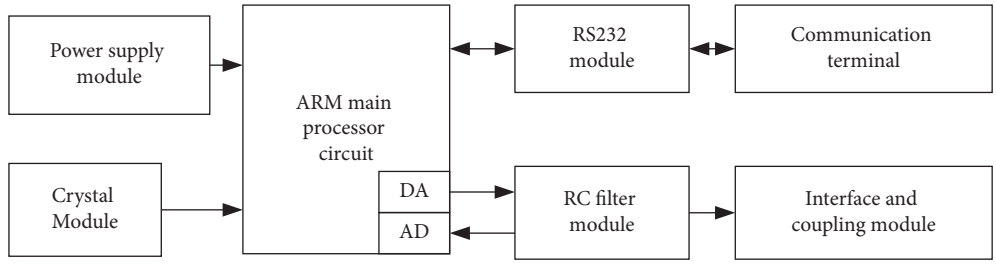

Figure 6: General block diagram of the system hardware.

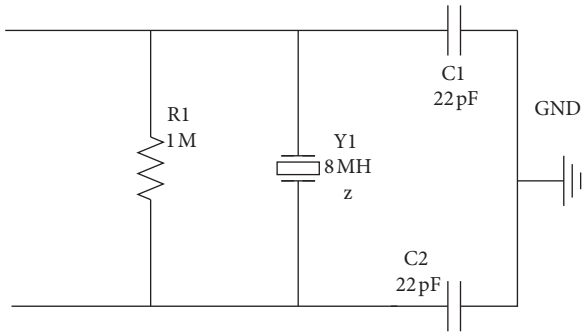

Figure 7: Crystal oscillator circuit of 8 M.

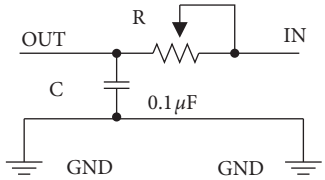

Figure 8: Low-pass RC filter circuit.

where v_{LED} denotes the DC voltage of the LED and $f(v_{\mathrm{LED}})$ denotes the DC voltammetric characteristic function of the LED. At the receiver end of a biased optical OFDM VLC system, the signal received by the photodetector PD can be expressed as follows:

$$r(n) = R_{\mathrm{PD}}\left[y(n) \otimes h_{\mathrm{c}}(n)\right] + z(n), \tag{8}$$

where R_{PD} is the responsiveness of the PD, $h_{\mathrm{c}}(n)$ is the equivalent VLC system channel gain, $\otimes$ represents the convolution operation, and $z(n)$ is the zero-mean additive white Gaussian noise (AWGN). At the receiver end of a biased optical OFDM VLC system, the photodetector PD converts the received optical signal into an electrical signal and then performs the opposite operation to the transmitter end, resulting in a binary signal.

5.3. Block Diagram of the Overall Hardware Architecture. In order to implement the functions of a biased optical OFDM VLC system, a high-performance processor is required for forward and inverse Fourier transform operations. The S3C6410 processor, based on the high-performance 32 bit ARM1176JZF-S core, was chosen after taking into account performance and cost factors. The ARM processor has lower power consumption and a rich peripheral interface, which is more suitable for OFDM system hardware implementation. The overall block diagram of the system hardware is shown in Figure 6.

5.4. Crystal Circuit Design. The system is powered directly by AC 220 V. In addition, to provide a stable 8 M frequency square wave output, the core S3C6410 processor has an external 8 M crystal oscillator as the clock signal, as shown in Figure 7.

5.5. Passive Low-Pass RC Filter Circuit Module. In order to perform the necessary noise filtering on the output signal of the system, a passive low-pass RC filter is externally connected to the DA/AD interface, and the modulated OFDM signal frequency f is expressed as follows:

$$f = \frac{1}{(2\pi RC)}, \tag{9}$$

where C indicates the capacitance in this circuit. C is set to 0.1 μF in this system. R indicates the resistor in this circuit. A potentiometer is used in this system so that it can be adjusted as required. The low-pass RC filter circuit is shown in Figure 8.

5.6. Design of Leading and Windowing Functions. Energy efficiency is an important indicator in optical communication systems and needs to be maximised wherever possible. Therefore, the improvement of energy efficiency has become a key issue in optical communication systems. Therefore, this paper attempts to design the lead and window functions used in the physical layer based on the biased optical OFDM VLC system to transmit signals only in the over-zero region, so as to improve the communication energy efficiency of the system as much as possible while ensuring the system bandwidth.

In this paper, we try to use only 1/3 of the band, that is, near the over-zero zone, for the transmission of the signal during the entire photoelectric conversion cycle. Because this zone has the lowest background noise and interference, it is the most desirable time slot for communication. Therefore, a constant envelope zero autocorrelation sequence is used as a leading code in order to shorten the frame length. Specifically, a Zadoff–Chu sequence was used, the expression of which is as follows:

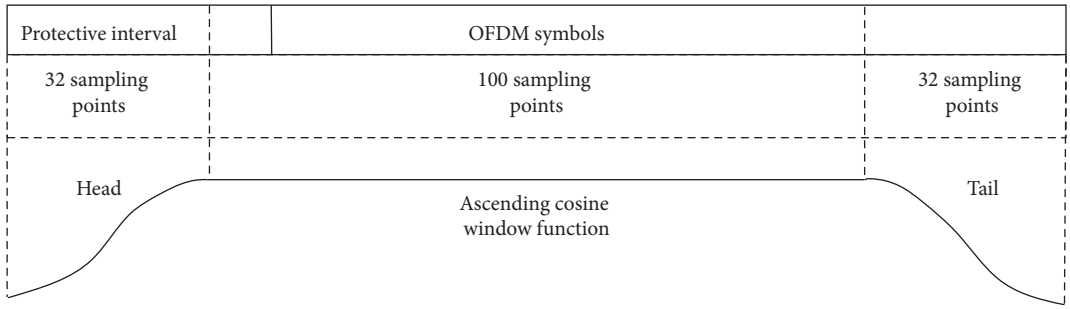

Figure 9: Time domain waveform of the window function.

$$a_k = \begin{cases} \exp\left[j2\pi \dfrac{M}{N}\left(\dfrac{k(k+1)}{2} + qk\right)\right], N \text{ is odd.} \\ \\ \exp\left[j2\pi \dfrac{M}{N}\left(\dfrac{k^2}{2} + qk\right)\right], N \text{ is even.} \end{cases}, \quad (10)$$

where $k = 0, 1, \ldots, N-1$, N denotes the length of the sequence, M is reciprocal to N, and q denotes a random integer.

The system was designed with a centre frequency of 421 kHz, and a Zadoff–Chu sequence ($N = 30$, $M = 29$, and $q = 15$) was chosen to meet the frame length parameters [29].

In order to window the OFDM signal with the aim of minimising spectral energy leakage, a rising cosine window is generally used, which is defined as follows:

$$w(t) = \begin{cases} 0.5 + 0.5 \cdot \cos\left(\dfrac{\pi + t\pi}{(\beta T_s)}\right) & 0 \le t \le \beta T_s \\ \\ 1.0 & \beta T_s \le t \le T_s \\ \\ 0.5 + 0.5 \cdot \cos\left(\dfrac{(t - T_s)\pi}{(\beta T_s)}\right) & T_s \le t \le (1+\beta) T_s \end{cases}, \quad (11)$$

where β indicates the roll-off factor of the added window and T_s indicates the cycle length of the symbol.

In this system, $T_s = 1{,}174$. The raised cosine window is calculated by discrete time.

$$w(n) = \begin{cases} 0.5 - 0.5 \cdot \cos\left(\dfrac{\pi \cdot n}{32}\right) & 0 \le n \le 31 \\ \\ 1 & 32 \le n \le 1141 \\ \\ 0.5 - 0.5 \cdot \cos\left(\dfrac{\pi \cdot (n - 1174)}{32}\right) & 1142 \le n \le 1173 \end{cases}. \quad (12)$$

Therefore, the time domain waveform diagram of the window function used in this system is shown in Figure 9.

DBPSK modulation is used to implement the subcarrier modulation, and the frame length of the system is defined as follows:

$$\begin{aligned} T_{\text{frame}} &= \frac{N_{\text{FFT}} \cdot N_{\text{pre}} + (N_{\text{FFT}} + N_{\text{CP}} - N_{\text{window}}) \cdot (N_{\text{FCH}} + N_{\text{DATA}})}{f_s} \\ &= [1024 \times 3 + (1024 + 120 - 32) \times 5] \div \left(2.0 \times 10^6\right) \\ &= 3.253\,(\text{ms}), \end{aligned} \quad (13)$$

where N_{DATA} indicates the length of the DATA field information, N_{CP} indicates the number of useful subcarriers, N_{window} indicates the number of window cover points, N_{FCH} indicates the number of frame control header symbols, N_{FFT} indicates the number of fast Fourier transform points, N_{pre} indicates the number of leading symbols, and f_s indicates the sampling frequency.

The results from equation (11) show that the frame length of the system is significantly reduced. Combined with the OFDM symbol power spectrogram after windowing, the planned over-zero zone signal transmission is accomplished, thus effectively improving the energy efficiency of data communication.

6. Experimental Results and Analysis

6.1. Experimental Setup. The commissioning process for the transmitter and receiver circuits of the RGB-LED VLC system is as follows:

(1) First of all, the mechanical performance of each module should be debugged and tested; check whether each module component is well connected to each other, especially whether the installed components are normal

(2) Check the component power supply and detect if the module is working properly

(3) Debugging program: burn the written software program into the microcontroller to see if the program makes each module perform the desired function

(4) Overall system debugging: debug the transmitter and receiver circuits and observe whether the output waveforms of each port meet the circuit requirements through an oscilloscope

After the selection and commissioning of the above system components, the prototype system was finally

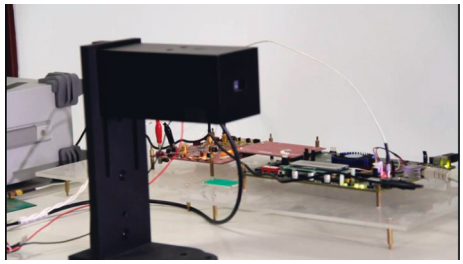

Figure 10: Indoor RGB-LED VLC system hardware.

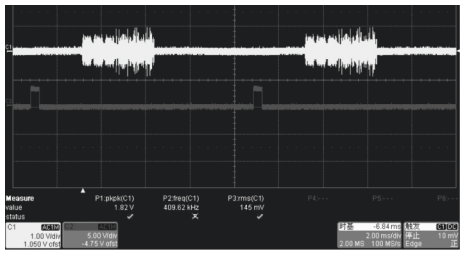

Figure 11: Time domain waveform of the frame signal.

Table 3: Relationship between voltage drop and light intensity.

LED voltage drop (V)	Light intensity (lux)
2.66	143
2.78	648
2.89	1,191
2.96	1,685
3.02	2,210
3.13	3,012
3.24	4,172
3.30	5,309

completed. The hardware of the indoor RGB-LED VLC system is shown in Figure 10.

6.2. Communication Trials and Performance Tests. Next, the system performance will be tested in terms of the driving voltage, communication distance, light intensity, and BER. As testing the three lights separately would be somewhat repetitive, a single RGB-LED light source is chosen for testing in this paper. The following experimental tests were carried out using blue light as an example. The time domain waveform of the received frame signal at the receiver side is shown in Figure 11. We can see that one frame of the oscilloscope represents 40 μs and the average period is 3 frames, so the signal frequency is 8.4 kHz.

The results of the drive voltage and light intensity tests are shown in Table 3. As can be seen from Table 3, the voltage drop of the LED is proportional to the light intensity. However, due to the limited carrying voltage of the LED, the maximum light intensity of the LED used in this system is 5,390 lux.

The relationship between the voltage intensity of the blue LED at different distances and the BER is shown in Table 4.

The BER is lowest when the light intensity at the transmitter is 3,370 lux, so the optimum communication

Table 4: Distance-light intensity-BER relationship.

Distance (cm)	Light intensity (lux)	BER ($\times 10^{-3}$)
1	4,220	5.2
1.5	3,370	4.8
2	2,830	5.1
2.5	2,520	5.4
3	1,952	6.1
3.5	1,392	6.7
4	1,342	6.7
4.5	976	8.6
5	811	9.8

Table 5: System throughput test results.

Distance (cm)	Uplink throughput (Mbps)	Downlink throughput (Mbps)
1	23	24
1.5	24	25
2	22	23
2.5	20	21
3	16	17
3.5	11	12
4	6	7
4.5	3	4
5	1	2

state for this system is a transmission distance of 1.5 cm and a light intensity of 3,370 1ux. The throughput of this system at distances from 1 to 5 cm was tested using a network tester, and the results are shown in Table 5.

With a packet size of 128 bytes and a throughput load of 80%, the system delay performance was tested using a network tester at different distances, and the results are shown in Table 6.

With a packet size of 128 bytes and a throughput load of 80%, the system delay performance was tested using a network tester at different distances, and the results are shown in Table 7.

As a key metric for communication systems, reliability verification is a necessary component of test validation. Using the Monte Carlo method, the ARM-based indoor RGB-LED VLC system was tested 20 times with a data transmission size of 500 frames each. The average BER results of the system are shown in Figure 12.

Overall, at a distance of 5 cm, the system has a packet loss rate of 0%, a maximum average delay of 36 ms, and a maximum throughput of 25 Mbps, all of which meet the actual broadband access requirements. In addition, Figure 12 shows that after −5 dB, the average BER of the system decreases significantly with the increase of the signal-to-noise ratio up to 4.8×10^{-3} level, which can effectively ensure the reliability of communication.

In terms of system energy efficiency, the maximum value of energy efficiency is obtained in the scenario of a horizontal LED layout when the horizontal distance $r = 1.5$ cm, which is in line with the above results (lowest BER). This is because at this position the LEDs are facing the PD and the PD can

Table 6: System delay test results.

Distance (cm)	Uplink delay (ms)	Downlink delay (ms)
1	11	9
1.5	15	13
2	21	18
2.5	27	25
3	36	34
3.5	41	42
4	48	49
4.5	57	56
5	68	65

Table 7: System packet loss rate test results.

Distance (cm)	Uplink delay (%) (ms)	Downlink delay (%) (ms)
1	0	0
1.5	0	0
2	0	0
2.5	0	0
3	0	0
3.5	0.01	0.01
4	0.01	0.01
4.5	0.01	0.01
5	0.01	0.01

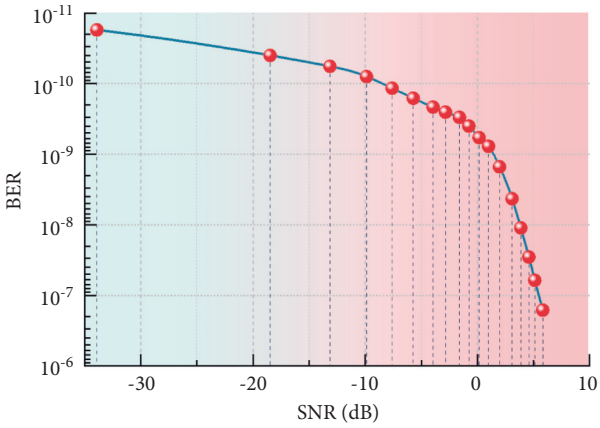

Figure 12: Average BER of the RGB-LED VLC system.

receive most of the light energy; therefore, the maximum system energy efficiency is obtained at this position. In practical system design, the horizontal distance r can be configured according to the requirements of the different layouts of the LEDs. It should be noted, however, that the smaller the horizontal distance r, the more difficult it is to implement a biased light OFDM system.

7. Conclusion

This paper presents an ARM-based indoor RGB-LED VLC system. RGB-LEDs are combined with OFDM technology to implement a VLC system in order to improve the system transmission bandwidth. Based on the characteristics of the light source of the OFDM-based VLC system, the leading and window functions used in the optical network transceiver module are designed to improve the communication energy efficiency of the system. In addition, an embedded ARM platform was built for OFDM modulation and demodulation to achieve low-cost network access for the visible light system. Experimental results verify the feasibility of the system. The maximum energy efficiency was obtained in the LED horizontal layout scenario when the horizontal distance $r = 1.5$ cm, and the BER was only 4.8×10^{-3}. Overall, at a distance of 5 cm, the system had a packet loss rate of 0%, a maximum average delay of 36 ms, and a maximum throughput of 25 Mbps, all of the above performance indicators meeting the actual broadband access requirements. Further research will be carried out on how to design good LED and PD arrays while increasing the transmission distance and ensuring system stability.

Data Availability

The experimental data used to support the findings of this study are available from the corresponding author upon request.

Conflicts of Interest

The authors declare that they have no conflicts of interest to report regarding the present study.

Acknowledgments

This work was supported by (1) Science and Technology Innovation Strategy Projects of Guangdong Province: Research on High Reliable Transmission Technology in an Indoor Visible Light Communication System (pdjh2022b1030) and Design of Full-Color Direct Display MiniLED Display Module Using Flip-Chip COB Package (pdjh2022b1026); (2) Special Projects in Key Fields of General Colleges and Universities of Guangdong Province: Design of Full-Color Direct Display MiniLED Display Module Using Flip-Chip COB Package (2020ZDZX3091) and Design and Research of Elevator Absolute Positioning System Based on Optical Communication and Artificial Neural Network (2021ZDZX1133); (3) Engineering Technology Research Center of General Colleges and Universities of Guangdong Province, Intelligent Terminal Application Engineering Technology Development Center (2021GCZX016); (4) Major Nature Science Projects of Guangdong Colleges and Universities: Study on Welding Process Control Based on the Morphology of Molten Pool (2019GZDXM016) and Intelligent Terminal and Intelligent Manufacturing Special Projects of Dongguan Vocational and Technical College: Scientific backbone (ZXE003); (5) SMT Component Placement Defect Recognition System Based on Deep Neural Network (ZXF005); and (6) Research of 5G Terminal OTA Performance Automatic Test System, Dongguan Science and Technology Commissioner Project (20201800500652).

References

[1] H. W. Chen, J. H. Lee, and B. Y. Lin, "Liquid crystal display and organic light-emitting diode display: present status and

future perspectives," *Light: Science & Applications*, vol. 7, no. 3, pp. 17–25, 2018.

[2] L. G. Langella, P. Silva, and L. Costa-Santos, "Photobiomodulation versus light-emitting diode (LED) therapy in the treatment of temporomandibular disorder: study protocol for a randomized, controlled clinical trial," *Trials*, vol. 19, no. 1, pp. 71–79, 2018.

[3] H. Zhong, T. Duan, H. Lan, M. Zhou, and G. Fei, "Review of low-cost photoacoustic sensing and imaging based on laser diode and light-emitting diode," *Sensors*, vol. 18, no. 7, pp. 2264–2278, 2018.

[4] J. Alexandersen, O. Sigmund, K. E. Meyer, and B. S. Lazarov, "Design of passive coolers for light-emitting diode lamps using topology optimisation," *International Journal of Heat and Mass Transfer*, vol. 122, pp. 138–149, 2018.

[5] C. Soeiro, D. Bitton, B. A. Maria, Z. L. Fernando, and N. A. Nikele, "Light Emitting Diode (LED) therapy reduces local pathological changes induced by *Bothrops asper* snake venom," *Toxicon*, vol. 152, pp. 95–102, 2018.

[6] W. Chen, Y. Zhuang, and W. Le, "Color-tunable and high-efficiency dye-encapsulated metal-Organic framework composites used for smart white-light-emitting diodes," *ACS Applied Materials & Interfaces*, vol. 10, no. 22, pp. 18910–18917, 2018.

[7] C. Qian, H. Zhang, J. Dai, Z. Shuang, and S. Wang, "Enhanced the Optical power of AlGaN-based deep ultraviolet light-emitting diode by optimizing mesa sidewall angle," *IEEE Photonics Journal*, vol. 10, pp. 1–7, 2018.

[8] H. L. Ji, H. C. Kang, and J. W. Jo, "Concentrated perovskite photovoltaics enable minimization of energy loss below 0.5 eV under artificial light-emitting diode illumination," *International Journal of Energy Research*, vol. 46, no. 4, pp. 5260–5268, 2022.

[9] A. E. Alexei, C. Hoepfner, and Panaccione, "Organic light emitting diode unit and method for manufacturing the same," *Metal Industries Research & Development Centre*, vol. 625, no. 5, pp. 135–148, 2018.

[10] G. S. Prasad and S. B. Kumar, "Shear bond strength of a bracket-bonding system cured with a light-emitting diode or halogen-based light-curing unit at various polymerization times," *Clinical, Cosmetic and Investigational Dentistry*, vol. 10, pp. 61–67, 2018.

[11] D. Xie, Y. L. Li, G. F. Wang, J. Jiang, and L. R. Sun, "Ultraviolet light-emitting diode irradiation induces reactive oxygen species production and mitochondrial membrane potential reduction in HL-60 cells," *Journal of International Medical Research*, vol. 49, no. 5, pp. 33–41, 2021.

[12] B. O. Rothbaum, M. Price, and T. Jovanovic, "A randomized, double-blind evaluation of D-cycloserine or alprazolam combined with virtual reality exposure therapy for post-traumatic stress disorder in Iraq and Afghanistan War veterans," *American Journal of Psychiatry*, vol. 171, no. 6, pp. 640–648, 2014.

[13] H. A. Elessawy, W. H. Borhan, and N. A. Ghozlan, "Effect of light-emitting diode irradiation on chronic nonhealed wound after below-knee amputation," *The International Journal of Lower Extremity Wounds*, vol. 20, no. 3, pp. 251–256, 2021.

[14] T. Grünbaum, S. Bange, J. Wei, and A. E. Leung, "Measuring the magnetic field amplitude of rf radiation by the quasistatic magnetic field effect in Organic light-emitting diodes," *Physical Review Applied*, vol. 15, no. 6, pp. 112–129, 2021.

[15] R. Winzenrieth, M. S. Ominsky, Y. Wang, and L. Humbert, "Differential effects of abaloparatide and teriparatide on hip cortical volumetric BMD by DXA-based 3D modeling," *Osteoporosis International*, vol. 32, no. 6, pp. 33–45, 2021.

[16] F. Radicioni, A. Stoppini, and G. Tosi, "Necropolis of Palazzone in Perugia: geomatic data integration for 3D modeling and geomorphology of underground sites," *Transactions in GIS*, vol. 25, no. 5, pp. 149–160, 2021.

[17] A. N. Kumar, V. Jadhav, R. Jawalekar, P. Akhare, and S. Gosavi, "Light emitting diode mediated photobiomodulation therapy in orthodontics - a review of contemporary literature," *Journal of Evolution of Medical and Dental Sciences*, vol. 10, no. 32, pp. 2672–2679, 2021.

[18] H. Xiao, R. Wang, G. He, Z. Lv, and K. Wang, "4 Mb/s under 3-m transmission distance using quantum dot light-emitting diode and NRZ-OOK modulation," *Optics Letters*, vol. 45, no. 6, pp. 83–92, 2020.

[19] Y. Wang, Y. Wang, N. Chi, J. Yu, and H. Shang, "Demonstration of 575-Mb/s downlink and 225-Mb/s uplink bi-directional SCM-WDM visible light communication using RGB LEDs and phosphor-based LEDs," *Optics Express*, vol. 21, no. 1, pp. 1203–1208, 2013.

[20] H. Marshoud, S. Muhaidat, and P. C. Sofotasios, "Optical non-orthogonal multiple access for visible light communication," *IEEE Wireless Communications*, vol. 25, no. 2, pp. 82–88, 2018.

[21] R. Ferreira, E. Xie, J. Mckendry, S. Rajbhandari, and H. Chun, "High bandwidth GaN-based micro-LEDs for multi-gb/s visible light communications," *IEEE Photonics Technology Letters*, vol. 28, no. 19, pp. 2023–2026, 2019.

[22] H. Chen, W. Guan, S. Li, and Y. Wu, "Indoor high precision three-dimensional positioning system based on visible light communication using modified genetic algorithm," *Optics Communications*, vol. 413, pp. 103–120, 2018.

[23] M. Fu, W. Zhu, and Z. Le, "Improved visible-light-communication positioning algorithm based on image sensor tilting at room corners," *IET Communications*, vol. 12, no. 10, pp. 1201–1206, 2018.

[24] N. Chi, *The Transmitter of the Visible Light Communication System*, 2018.

[25] J. Y. Wang, L. Cheng, J. B. Wang, Y. Wu, M. Lin, and J. Cheng, "Physical-layer security for indoor visible light communications: secrecy capacity analysis," *Communications, IEEE Transactions on*, vol. 66, no. 12, pp. 6423–6436, 2018.

[26] W. Guan, X. Chen, and M. Huang, "High-speed robust dynamic positioning and tracking method based on visual visible light communication using Optical flow detection and bayesian forecast," *IEEE Photonics Journal*, vol. 10, no. 3, pp. 1–22, 2018.

[27] W. Guan, Y. Wu, C. Xie, L. Fang, X. Liu, and Y. Chen, "Performance analysis and enhancement for visible light communication using CMOS sensors," *Optics Communications*, vol. 410, pp. 531–545, 2018.

[28] C. W. Chow, R. J. Shiu, and Y. C. Liu, "Non-flickering 100 m RGB visible light communication transmission based on a CMOS image sensor," *Optics Express*, vol. 26, no. 6, pp. 7079–7086, 2018.

[29] R. Ji, S. Wang, Q. Liu, and W. Lu, "High-speed visible light communications: enabling technologies and state of the art," *Applied Sciences*, vol. 8, no. 4, pp. 589–597, 2018.